ADVANCED ENGINEERING MATERIALS

DOI: 10.1002/adem.201500607

An Active Microarchitectured Material that Utilizes Piezo Actuators to Achieve Programmable Properties**

By *Yuanping Song, Peter C. Dohm, Babak Haghpanah, Ashkan Vaziri* and *Jonathan B. Hopkins**

In this paper, a new microarchitectured material is introduced that consists of a large periodic lattice of small compliant unit cells (i.e., <5 mm) that are independently controlled using piezo actuators, sensors, and microprocessors embedded within each cell. This material exhibits desired bulk properties according to control instructions that are programmed and uploaded to the material's microprocessors. Analytical methods are used to identify optimal design instantiations of the material that achieve programmable properties over ranges of strain as high as 9.1% or achieve any desired stiffness over ranges of externally applied stresses as high as 10.6 MPa without failing. A macro-scale 2D version of the material's cell is fabricated and controlled to achieve desired stiffness values.

Unlike most microarchitectured materials[1,2] that passively exhibit their bulk properties based solely on their microstructure's topology and constituent material properties, the proposed material of this paper (Figure 1) actively exhibits its properties primarily from its internal piezo actuators, which are driven according to control instructions. Thus, if designers wish to achieve different combinations of desired properties (e.g., Young's Modulus, Poisson's ratio, density, and damping coefficient), they do not need to redesign or refabricate the mechanical infrastructure of their initial design, but can simply reprogram and upload new control instructions to the existing design such that the different combinations of bulk lattice properties can be achieved. And, since such control instructions can be altered and uploaded in real-time using a centralized master controller, desired combinations of properties can be actively and continuously tuned or maintained over appreciable deformations on demand. The proposed material can also achieve extreme mechanical properties that cannot be achieved by naturally occurring materials, composites, or other passive microarchitectured materials because the proposed material is energized by a power source (e.g., batteries or an external power line) that can significantly amplify the material's response to mechanical loads.

Some materials already exist with mechanical properties that can be actively tuned.[3] The stiffness properties of a number of homogeneous solid materials (e.g., ceramics,[4] polymers,[5] metallic oxides,[6] and shape memory alloys[7,8]) can be tuned by actively changing their temperature. More advanced materials that utilize different means of actuation have been developed to achieve a substantially larger range of tunable stiffness. Magnetic fields have been used to stiffen elastomers loaded with magnetic particles[9,10] as well as soft composites embedded with magnetorheological fluids.[11] Electricity has been used to electrostatically increase the stiffness of beams in bending[12,13] as well as lower the stiffness of composites embedded with low-melting-point metals via resistance heating.[14] Hydraulic pressure has also been used to stiffen composites filled with fluid[15] and pneumatic pressure has been used to stiffen structures via particle jamming.[16,17] A microarchitectured material design was recently proposed that utilizes electromagnetic locks to achieve discrete stiffness values, which approach continuity as the number of on-off locks within the lattice increases.[18] A key difference between these materials and the material proposed here is that the proposed material can be programmed to exhibit desired combinations of multiple

[*] *Prof. J. B. Hopkins, Dr. Y. Song, Dr. P. C. Dohm, Dr. B. Haghpanah*
Department of Mechanical and Aerospace Engineering, University of California, Los Angeles, Los Angeles, California 90095, USA
E-mail: hopkins@seas.ucla.edu
Prof. A. Vaziri
Department of Mechanical and Industrial Engineering, Northeastern University, Boston, Massachusetts 02115, USA

[**] *This work was primarily supported by the Air Force Office of Science Research under award number FA9550-15-1-0321. Program officer Byung "Les" Lee is gratefully acknowledged. NSF-CAREER grant number CMMI-1149750 (AV) is also acknowledged. Y. Song and Prof. J. B. Hopkins contributed equally to this work. (Supporting Information is available online from Wiley Online Library or from the author).*

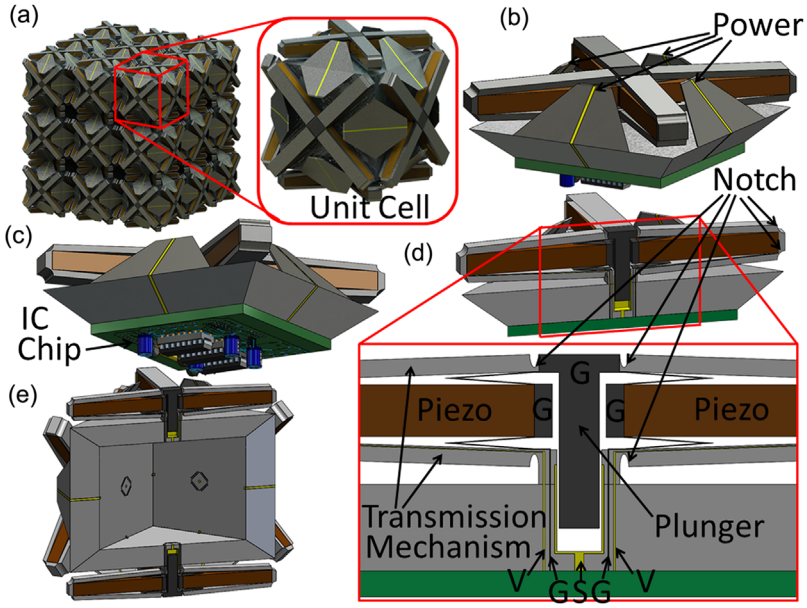

Fig. 1. (a) Active microarchitectured material lattice design, (b) and (c) its cell's repeated sector, (d) a cross-section of the sector, and (e) a cross-section of the unit cell.

properties simultaneously (e.g., Young's Modulus, Poisson's ratio, density, and damping coefficient) that can be maintained at constant values over appreciable deformations or actively tuned in a purely continuous way according to instructions uploaded within independently controlled unit cells. Such capabilities would impact advanced applications described in Supporting Information.

To understand how the proposed material achieves programmable properties, consider the periodic lattice of unit cells shown in Figure 1a. Each cube-shaped unit cell consists of the same sector design (Figure 1b and c) repeated six times within the cube. At the center of each unit cell is a microprocessor or integrated circuit (IC) chip, labeled in Figure 1c, that functions as the brain of each cell. Conductive lines, labeled "Power" in Figure 1b, run down the middle of trapezoid-shaped blade flexures to power the IC chip from an external source. The trapezoid-shaped blade flexures are designed to deform such that the unit cells are permitted to move with respect to one another as desired, while simultaneously constraining the unwanted relative shear and torsional motions. Note that the lattice's unit cells join together along the top faces of these trapezoid-shaped blade flexures as well as along the top face of each sector's plunger, labeled in Figure 1d. The cross-sectional view of Figure 1d details how the cell's IC chip could also be electrically grounded by an external source. The darkest gray regions, labeled "G" in Figure 1d, are conductive and are connected to an electrical ground. Note from the isometric view in the top portion of Figure 1d that the two bodies labeled "G" on either side of the plunger in the bottom portion of the same figure are joined together as part of the same rigid body with a hole down its central axis through which the plunger is designed to translate. Each sector's four piezo actuators, labeled "Piezo" in Figure 1d, span between this electrically grounded body at one end and a different conductive electrode at their other end. These electrodes are wired directly to the cell's IC chip via the lines labeled "V" in Figure 1d. If the IC chip imparts a positive or negative voltage on these "V" lines, the piezo actuators will expand or contract causing the plunger to move down or up, respectively, due to the fact that the actuators are placed within a compliant transmission mechanism, labeled in Figure 1d. This transmission mechanism causes the displacement of the plunger to amplify the displacement of the actuators, while also causing the plunger's output force capability to attenuate the actuators' output force capability. This transmission effect is important because piezo actuators inherently exhibit abundant output force capabilities but do so over limited ranges of strain. Thus, by adjusting the geometry of the transmission mechanism, designers can tune the lattice such that it achieves a useful range of programmable properties over a large range of strains. Note also that the transmission mechanism utilizes notch flexures, labeled "Notch" in Figure 1d, which cause small localized regions of deformation that maximize the transmission efficiency of the mechanism by minimizing the amount of strain energy stored in the compliant structure. Notch flexures also enhance the design's functionality because they are less likely to cause failure due to buckling compared with other flexure element alternatives (e.g., blade or wire flexures). Note also that the axes of the design's piezo actuators are aligned along the diagonal directions of the cube-shaped unit cell's square faces. This alignment allows the piezo actuators to be as long as possible such that their range of expansion and contraction can be maximized. Although the four piezo actuators are used to drive the sector's plunger along its axis, a sleeve-like capacitive sensor that surrounds the plunger could be used to sense its relative displacement. As the electrically grounded plunger translates along its axis, the conductive region that surrounds the bottom-portion of the plunger, colored yellow in Figure 1d, could be used to supply the unit cell's IC chip with the necessary electrical signal to determine the plunger's relative displacement via the line labeled "S." With the ability to actuate and sense the relative displacement of each sector's plunger, the lattice's unit cells can independently control their interactions using closed-loop control as governed by the instructions uploaded within each unit cell's IC chip. Note from the cross-sectional view of each unit cell in Figure 1e that a large percentage of the design's volume is afforded to the IC chips as well as potential antennas, if wireless uploading of control instructions is desired, and/or batteries, if the material is intended to operate in the absence of an external power source. If such batteries are also rechargeable, the lattice could be recharged by cyclically loading the material's lattice

externally because the design's piezo actuators would reversibly generate electrical power as they are mechanically strained. And, although it may be possible to actively control the lattice such that it exhibits isotropic material properties, the geometry of each unit cell possesses the necessary nine planes of symmetry[19] to passively exhibit cubic material properties. Approaches for fabricating this proposed material are provided in Supporting Information.

The material operates primarily on principles of swarm robotics[20] in which an overall desired behavior (i.e., a bulk property) emerges from the interactions of many smaller entities (i.e., unit cells) that are programmed to obey simple instructions relating to the behavior of the other entities in the swarm (i.e., the lattice of unit cells). Suppose, for instance, every unit cell within a lattice is programmed such that when their plungers are displaced by their neighbor in a particular direction along their axes, the cell's piezo actuators are instructed to respond by pushing the plungers in the opposite direction. This simple set of instructions would cause the entire lattice to exhibit a higher Young's Modulus than the lattice would exhibit passively. If, however, the unit cells are programmed such that the piezo actuators instead responded to the displaced plungers by pulling in the same direction, the overall lattice would achieve a low, zero, or even negative Young's modulus. A discussion of different instructions that cause the material to exhibit other properties and/or combinations of these properties is provided in Supporting Information.

To determine what ranges of properties the lattice topology of Figure 1 can be programmed to achieve, the geometry of each unit cell within the lattice is simplified such that each cell can be defined by five independent parameters labeled in Figure 2 (i.e., P, Q, H, e, and U). Optimal values for these parameters can be calculated by modeling each sector as beam elements that join together at rigid nodes, shown dark gray in Figure 2a. Suppose the beams labeled "Silicon" in Figure 2a possess a Young's modulus of 190 GPa, a shear modulus of 75 GPa, and a yield strength of 7 GPa. Suppose also the piezo actuator beams, labeled "Piezo (PZT-5H)," possess a Young's modulus of 43 GPa, a shear modulus of 16 GPa, a yield strength of 76 MPa, a maximum positive electric field of 2 kV mm^{-1}, a maximum negative electric field of -0.3 kV mm^{-1}, and an axial charge constant of 0.64 nm V^{-1}. The maximum negative and positive strain values that can be achieved by arbitrarily large lattices consisting of such unit cells are plotted in Figure 2b for almost one million different unit cell design instantiations. These design instantiations, shown as individual blue dots in Figure 2b, were generated by conducting a sweep of all the independent design parameters within one of the lattice's repeating unit cells starting from a smallest allowable feature size and incrementing each parameter small amounts until the largest geometrically

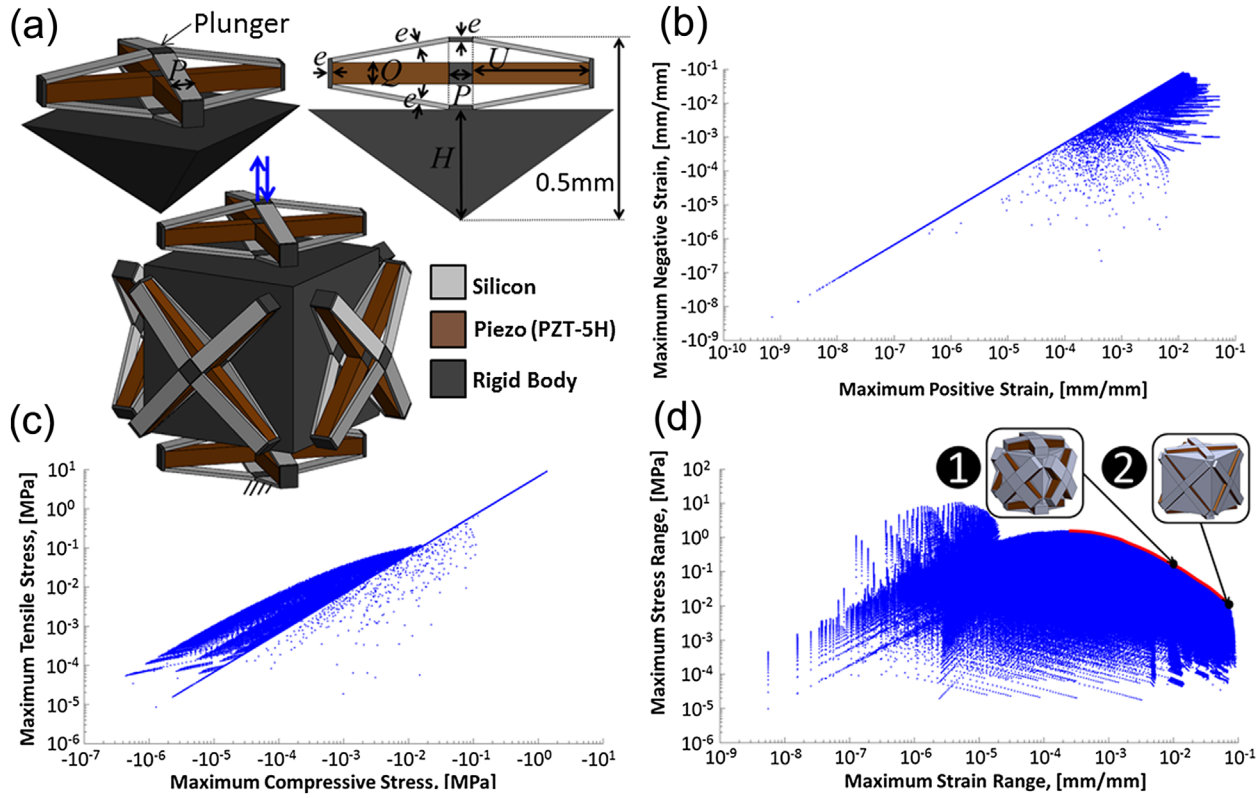

Fig. 2. (a) Simplified unit cell topology defined by five independent parameters, (b) a plot of the maximum negative and positive strains for every design instantiation of the cell's topology using an exhaustive sweep of the five parameters, (c) a plot of the maximum tensile and compressive stresses for the same design instantiations, and (d) a plot of the maximum stress and strain ranges for the same design instantiations showing two designs that lie along the optimal design curve.

Table 1. Finite element verification of the analytical predictions pertaining to design (1) from Figure 2d with P = 0.190 mm, Q = 0.090 mm, H = 0.310 mm, e = 0.011 mm, and U = 0.290 mm.

	Analytical calculations	Finite element results	Percent error
Maximum positive strain	0.14%	0.15%	6.67%
Maximum negative strain	−0.95%	−1.05%	9.52%
Maximum tensile stress	0.129 MPa	0.121 MPa	6.61%
Maximum compressive stress	−0.0194 MPa	−0.0181 MPa	7.18%

Table 2. Finite element verification of the analytical predictions pertaining to design (2) from Figure 2d with P = 0.120 mm, Q = 0.040 mm, H = 0.420 mm, e = 0.004 mm, and U = 0.470 mm.

	Analytical calculations	Finite element results	Percent error
Maximum positive strain	0.95%	0.99%	4.04%
Maximum negative strain	−6.28%	−6.58%	4.56%
Maximum tensile stress	0.00843 MPa	0.00827 MPa	1.93%
Maximum compressive stress	−0.00126 MPa	−0.00124 MPa	1.63%

compatible feature sizes were reached. The details of this parameter sweep are discussed in Supporting Information. The lattice's maximum negative and positive strain values were determined by calculating the largest distance the top face of the plunger, labeled in Figure 2a, could be displaced by the piezo actuators down and up without causing any elements within the sector to yield, buckle, or collide, and then divide these displacements by the sector height (i.e., 0.5 mm). The plunger displacements were calculated using the theory provided in Supporting Information. The maximum tensile and compressive stresses that can be resisted by the piezo actuators within the repeating unit cells of an arbitrarily large periodic lattice such that each unit cell's plungers do not displace without causing any elements within each unit cell design to yield, buckle, or collide are plotted in Figure 2c for the same design instantiations plotted in Figure 2b. These stresses were also calculated using the theory provided in Supporting Information. They are significant because they represent the ranges of loading stresses between which the entire lattice could be programmed to respond with any desired stiffness. Note that the lattice could still achieve a programmable stiffness if it were loaded with stresses outside of this range, but the resulting ranges of achievable stiffness would be reduced to finite amounts. Note also that although the strain and stress values in Figure 2b and c were plotted for large lattices that consist of 1 mm-sized unit cells, these strain and stress values are independent of both the number of unit cells within the lattice and the size of those unit cells. Optimal design instantiations can be identified by plotting the maximum stress ranges (i.e., the maximum compressive stresses subtracted from the maximum tensile stresses of Figure 2c) against the maximum strain ranges (i.e., the maximum negative strains subtracted from the maximum positive strains of Figure 2b) as shown in Figure 2d.

The optimal design instantiations with the largest ranges of maximum stresses and maximum strains lie along the curve shown red in Figure 2d. Two sample designs from this curve are labeled (1) and (2) in Figure 2d. Their predicted performance calculated via the analytical method of this paper is provided in Table 1 and 2, respectively. This performance was verified using finite element analysis (FEA) as provided in the same tables. Note that the design with larger nodes (i.e., design (1)) possesses more error because the analytical method of this paper models these nodes, shown dark gray in Figure 2a, as rigid bodies.

A 2D version of the 3D lattice of Figure 1 is shown in Figure 3a. A macroscale unit cell from this lattice was fabricated as a proof of concept (Figure 3b) and programmed to exhibit different constant stiffness values, which manifest as the slopes of the linear trends shown in Figure 3c, over a 0.5% strain. An Instron testing machine was used to collect the data plotted in Figure 3c. Details pertaining to the design, fabrication, and control of the cell shown in Figure 3b are provided in Supporting Information.

In summary, this paper proposes a new microarchitectured material that consists of independently controlled unit cells with microprocessors that can be programmed to drive piezo actuators in a controlled fashion such that the overall lattice

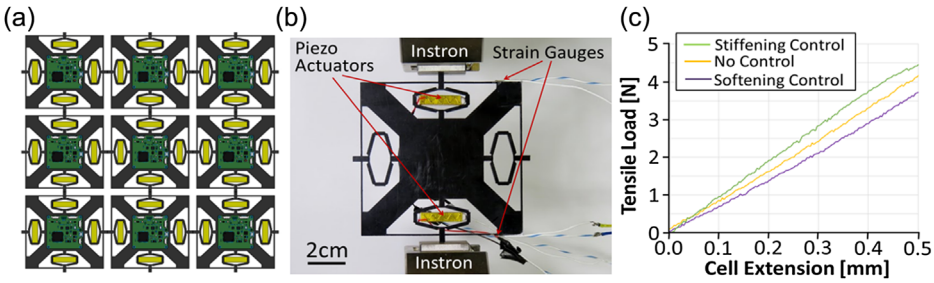

Fig. 3. (a) A 2D version of the design, (b) a unit cell prototype tested using an Instron machine, and (c) a plot demonstrating that the unit cell can be programmed to exhibit a desired constant stiffness (i.e., the slope of the tensile load vs. cell extension lines) via control over a strain of 0.5%.

exhibits desired bulk properties. Analytical methods are created to rapidly calculate and optimize the material's ranges of achievable programmable properties and a macro-scale 2D version of the unit cell design was fabricated and controlled to achieve desired stiffness values.

Article first published online: March 29, 2016
Manuscript Revised: March 14, 2016
Manuscript Received: December 1, 2015

[1] L. Valdevit, A. J. Jacobsen, J. R. Greer, W. B. Carter, *J. Am. Ceram. Soc*. **2011**, *94*, 15.
[2] J. Xiong, R. Mines, R. Ghosh, A. Vaziri, L. Ma, A. Ohrndorf, H. J. Christ, L. Wu, *Adv. Eng. Mater.* **2015**, *17*, 1253.
[3] R. Kornbluh, H. Prahlad, R. Pelrine, *Smart Struct. Mater. 2004 Ind. Commer. Appl. Smart Struct. Technol*. **2004**, *5388*, 372.
[4] W. Li, R. Wang, D. Li, D. Fang, *Phys. Res. Int*. **2011**, *2011*, 1.
[5] R. Li, J. Jiao, *Int. J. Microcircuits Electron. Packag*. **2000**, *23*, 456.
[6] J. B. Wachtman, W. E. Tefft, D. G. Lam, C. S. Apstein, *Phys. Rev.* **1961**, *122*, 1754.
[7] J. Rossiter, K. Takashima, F. Scarpa, P. Walters, T. Mukai, *Smart Mater. Struct*. **2014**, *23*, 045007.
[8] M. R. R. Hassan, F. Scarpa, M. Ruzzene, N. A. A. Mohammed, *Mater. Sci. Eng. A* **2008**, *481–482*, 654.
[9] Z. Varga, G. Filipcsei, M. Zrínyi, *Polymer (Guildf)* **2006**, *47*, 227.
[10] S. Abramchuk, E. Kramarenko, D. Grishin, G. Stepanov, L. V. Nikitin, G. Filipcsei, A. R. Khokhlov, M. Zrínyi, *Polym. Adv. Technol*. **2007**, *18*, 513.
[11] C. Majidi, R. J. Wood, *Appl. Phys. Lett*. **2010**, *97*, 164104.
[12] A. Bergamini, R. Christen, B. Maag, M. Motavalli, *Smart Mater. Struct*. **2006**, *15*, 678.
[13] M. Henke, J. Sorber, G. Gerlach, Multi-layer beam with variable stiffness based on electroactive polymers. Proc. SPIE 8340, Electroactive Polymer Actuators and Devices (EAPAD) **2012**, 83401P (April 26, 2012); DOI:10.1117/12.915138.
[14] W. Shan, T. Lu, C. Majidi, *Smart Mater. Struct*. **2013**, *22*, 085005.
[15] Y. Shan, M. Philen, A. Lotfi, S. Li, C. E. Bakis, C. D. Rahn, K. W. Wang, *J. Intell. Mater. Syst. Struct*. **2008**, *20*, 443.
[16] E. Brown, N. Rodenberg, J. Amend, A. Mozeika, E. Steltz, M. R. Zakin, H. Lipson, H. M. Jaeger, *Proc. Natl. Acad. Sci*. **2010**, *107*, 18809.
[17] V. Trappe, V. Prasad, L. Cipelletti, P. N. Segre, D. A. Weitz, *Nature* **2001**, *411*, 772.
[18] B. Haghpanah, H. Ebrahimi, D. Mousanezhad, J. B. Hopkins, A. Vaziri, *Adv. Eng. Mater.* DOI:10.1002/adem.201500295.
[19] S. C. Cowin, M. M. Mehrabadi, *Appl. Mech. Rev.* **1995**, *48*, 247.
[20] E. Şahin, in *Swarm Robot*. Springer, Berlin Heidelberg **2005**, 10.
[21] J. B. Hopkins, K. J. Lange, C. M. Spadaccini, *J. Mech. Des*. **2013**, *135*, 061004.

